Simulation of 3D Mesoscale Structure Formation in Concentrated Aqueous Solution of the Triblock Polymer Surfactants (Ethylene Oxide)$_{13}$(Propylene Oxide)$_{30}$(Ethylene Oxide)$_{13}$ and (Propylene Oxide)$_{19}$(Ethylene Oxide)$_{33}$(Propylene Oxide)$_{19}$. Application of Dynamic Mean-Field Density Functional Theory

B. A. C. van Vlimmeren,† N. M. Maurits,† A. V. Zvelindovsky,* G. J. A. Sevink, and J. G. E. M. Fraaije*

Faculty of Mathematics and Natural Sciences, University of Groningen, Nijenborgh 4, 9747 AG Groningen, The Netherlands

Received June 16, 1998; Revised Manuscript Received October 29, 1998

ABSTRACT: We simulate the microphase separation dynamics of aqueous solutions of the triblock polymer surfactants (ethylene oxide)$_{13}$(propylene oxide)$_{30}$(ethylene oxide)$_{13}$ and (propylene oxide)$_{19}$(ethylene oxide)$_{33}$-(propylene oxide)$_{19}$ by a dynamic variant of mean-field density functional theory for Gaussian chains. This is the *first* 3D mesoscale model for the dynamic behavior of specific complex polymer solutions. Different mesoscale structures (micellar, hexagonal, bicontinuous, and lamellar and dispersed coexisting phases) are formed depending on composition. The numerical results are in good agreement with experiment. The intermediate hexagonal and bicontinuous phases of (ethylene oxide)$_{13}$(propylene oxide)$_{30}$-(ethylene oxide)$_{13}$ solution retain a rich defect structure. Concentrated solution (60%) of (propylene oxide)$_{19}$-(ethylene oxide)$_{33}$(propylene oxide)$_{19}$ shows the onset of macrophase separation, with small water droplets dispersed throughout the system. We confirm the experimental observation that the lamellar phase formation does not depend on the block sequence. Quenched from homogeneous state, the kinetics of each system consists of a fast local aggregation stage and subsequent slow rearrangement by defect annihilation. We conclude that the simulation method is a valuable tool for description of 3D morphology formation in a wide variety of complex polymer liquids.

Introduction

In a recent review,[1] it is remarked that "Polymers afford unique opportunities for detailed study of the thermodynamics of soft condensed matter, such as self-assembly processes and phase transitions". Concentrated aqueous mixtures of amphiphilic block copolymers are of special interest as they are intermediate between polymer melts and aqueous solutions of low molar mass surfactants. We study the behavior of aqueous solutions of polymer surfactants (ethylene oxide)$_{13}$(propylene oxide)$_{30}$(ethylene oxide)$_{13}$ (trade name Pluronic L64 or PL64) and (propylene oxide)$_{19}$(ethylene oxide)$_{33}$(propylene oxide)$_{19}$ (trade name Pluronic 25R4).[2−4] The PL64 surfactant has two outer hydrophilic blocks which can shield the hydrophobic block from contact with water. The 25R4 surfactant has the "inverse" sequence, where one hydrophilic middle block has a hydrophobic block on each side. Pluronic polymer surfactants find widespread application in a variety of industrial and academic colloidal systems.[2]

Our dynamic mean-field density functional model combines Gaussian mean-field statistics with a coarse-grained Ginzburg−Landau model for time evolution of conserved order parameters. This amounts to the application of time-dependent potential models for "pattern formation outside equilibrium".[5] In contrast to traditional phenomenological free energy expansion methods (Cahn−Hilliard,[6] Oono−Puri,[7] Flory−Huggins−de Gennes[8]), we do not truncate the free energy at a certain level, but rather retain the full polymer path integral by a numerical procedure.[9−20] Very recently, a few other groups also started to use this approach.[21,22] The theory of the dynamic density functional method can be traced back a few decades, and variants have in fact been reported in several classical textbooks (in Landau expansion format the theory is known as dynamic RPA).[23,24] Until recently, however, algorithms were of insufficient quality for reliable 3D calculations, and computer resources were too limited for manipulation of the gigabytes of numerical data involved in the simulations. As far as we know, this is the first demonstration of the application of the method to 3D mesoscale structure formation in *specific* polymer solutions, including the calculation of the full polymer path integral.

The repeated calculation of the polymer path integral is computationally more expensive than the integration of any of the traditional expansion models listed above. On the other hand, phenomenological free energies contain only the basic physics of the phase separation problem[12] and are not well suited to describe the rich phase behavior of complex industrial and biological systems. The extra computational cost of the path integral calculation is justified if by doing so the phase behavior of a specific system can be reproduced or even better can be predicted, without adjustment of parameters. Our dynamic theory lays in the general framework of self-consistent mean-field theory for polymers. Calculations of equilibrium polymer mixture/solution morphologies (statics) within this framework using path integral formalism can be found for example in refs 25 and 26.

† Also at: InterScale, Planetenlaan 413, 9742 HP Groningen, The Netherlands.

* Authors for correspondence.

10.1021/ma980947+ CCC: $18.00
Published on Web 01/20/1999

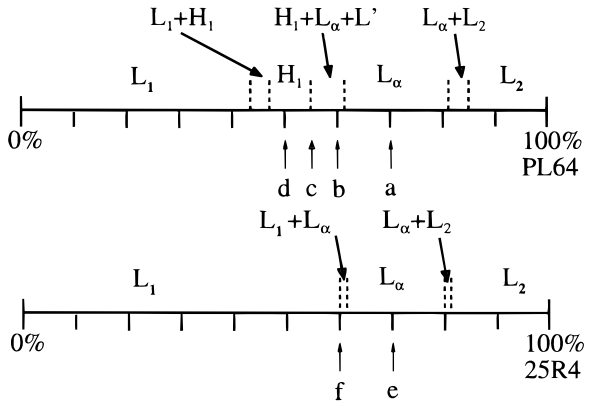

Figure 1. Experimental phase diagram of aqueous Pluronic polymer surfactant solution at 25 °C. (Data for PL64 are from ref 3 and from ref 49 for 25R4.) The concentrations are in polymer weight percentage, wt %. The observed microphases are shown at the top of each diagram. L_1, H_1, L′, L_α, and L_2 denote normal micellar, hexagonal, bicontinuous, lamellar, and water-lean continuous phase, respectively. The $H_1 + L_\alpha + L'$ region in Pl64 solution consists of smaller domains with less well-defined boundaries between L′, $H_1 + L'$, $H_1 + L_\alpha + L'$, and $L' + L_1$. Labels a−f refer to reported simulations. For PL64 solution (a) 70%, (b) 60%, (c) 55%, (d) 50%, and for 25R4 solution (e) 70%, (f) 60%.

In this paper we present simulations of microphase behavior in aqueous PL64 and 25R4 solutions by application of the 3D model. The experimental water−Pluronic phase diagrams[3,4] are partly reproduced in Figure 1. The polymer PL64 forms four different phases (micellar, hexagonal, bicontinuous, and lamellar) in a small 50−70% surfactant concentration interval. The polymer 25R4 forms only a lamellar mesoscale structure in concentrated solution.

We simulate the morphology formation by an instantaneous quench from homogeneous density distribution. The evolution of the mesoscale structures is followed directly from observation of 3D density fields. The time scale of phase separation is on the order of milliseconds−seconds. The final morphologies are not completely perfect but retain a rich defect structure due to the relatively short equilibration times. We reproduce the mesoscale structure formation and also two-phase regions in the two different polymer surfactant solutions using the same set of parameters. The phase boundaries are somewhat off; nevertheless, the results are in very good agreement with experiment. In the model both the 25R4 70% and PL64 70% solutions are lamellar (L_α), Pl64 60% solution is bicontinuous (L′), PL64 55% is hexagonal (H_1), and PL64 50% is micellar (L_1). We find tiny water droplets dispersed in the lamellar 25R4 60% solution, indicating the onset of macrophase separation. The lamellae orient perpendicular to the droplet−solution interface.

The background of the method is described extensively in a number of papers from our group.[9−20] The present paper is the first in a series devoted to the application of the dynamic density functional method to Pluronic polymer solutions. Simulations of sheared hexagonal phase of aqueous PL64 solutions are reported in ref 20.

Theory

A. Free Energy. We assume that the conformational distribution is in local equilibrium constantly on a time scale which is coarse-grained with respect to internal polymer relaxation times.[9] The Pluronic solutions are modeled as three-component compressible systems consisting of Gaussian chains in a mean-field environment. The three concentration fields ρ_{EO} (ethylene oxide), ρ_{PO} (propylene oxide), and ρ_w (water) are the independent order parameters. The free energy functional reads[10,12]

$$F[\rho] = F^{id}[\rho] + F^{coh}[\rho] + F^{comp}[\rho] \quad (1)$$

$$F^{id}[\rho] = -kT \ln \frac{\Phi_p^{n_p}\Phi_w^{n_w}}{n_p!\, n_w!} - \sum_I \int_V U_I(\mathbf{r})\, \rho_I(\mathbf{r})\, d\mathbf{r} \quad (2)$$

$$F^{coh}[\rho] = \frac{1}{2}\sum_{I,J} \int_{V^2} \epsilon_{IJ}(\mathbf{r} - \mathbf{r}')\, \rho_I(\mathbf{r})\, \rho_J(\mathbf{r}')\, d\mathbf{r}\, d\mathbf{r}' \quad (3)$$

$$F^{comp}[\rho] = \frac{\kappa_H}{2} \int_V \Big(\sum_I \nu_I(\rho_I(\mathbf{r}) - \rho_I^0)\Big)^2 d\mathbf{r} \quad (4)$$

where n_p (n_w) is the number of polymer (water) molecules, Φ is the intramolecular partition function, I is a component index (EO, PO, or w), and V is the system volume. The average concentration is ρ_I^0, and ν_I is the bead volume. F^{id} is the ideal free energy, given the external fields U_I. F^{coh} models the cohesive interactions with Gaussian kernels ϵ_{IJ}. F^{comp} accounts for the compressibility according to Helfand's penalty on high-density fluctuations.[13]

For each component the external potential is conjugate to the concentration fields via the appropriate density functional:

$$\rho_{PO}(\mathbf{r}) = \sum_s \delta^K_{PO,s} \rho_s \quad (5)$$

$$\rho_{EO}(\mathbf{r}) = \sum_s \delta^K_{EO,s} \rho_s \quad (6)$$

$$\rho_s(\mathbf{r}) = N_p \int_{V^N} \delta(\mathbf{r} - \mathbf{R}_s) e^{-\beta(H + \sum_{s'} U_{s'}(\mathbf{R}_{s'}))}\, d\mathbf{R}_1 ... d\mathbf{R}_N \quad (7)$$

$$\rho_w(\mathbf{r}) = N_w e^{-\beta U_w(\mathbf{r})} \quad (8)$$

where N_p and N_w are normalization constants,[27] N is the number of Gaussian beads in the polymer, and $\boldsymbol{R}_s$ is the position of bead s. $\delta^K_{X,s}$ is Kronecker's delta with value 1 if bead s is of type X and 0 otherwise. The Pluronic molecules are modeled as discrete strings of beads through the Edwards Hamiltonian H for Gaussian chains:

$$H \equiv \frac{3\beta^{-1}}{2a^2} \sum_{s=2}^{N} (\mathbf{R}_s - \mathbf{R}_{s-1})^2$$

B. Dynamics. The kinetic model consists of a set of stochastic diffusion equations with local kinetic coupling coefficients.[14] The diffusion equations are

$$\frac{\partial \rho_I}{\partial t} = M_I \nabla \cdot \rho_I \nabla \frac{\delta F}{\delta \rho_I} + \eta_I \quad (9)$$

where M_I is a mobility coefficient. The thermal noise η_I is distributed according to the fluctuation−dissipation theorem[15,28,29]

$$\langle \eta_I(\mathbf{r},t)\rangle = 0 \tag{10}$$

$$\langle \eta_I(\mathbf{r},t)\, \eta_J(\mathbf{r}',t')\rangle = -2kT\delta_{IJ}M_I\nabla\cdot\rho_I\,\nabla\delta(\mathbf{r}-\mathbf{r}')\,\delta(t-t') \tag{11}$$

It is possible to introduce more advanced nonlocal Rouse or reptation models for the kinetic coefficients[14,30−32] and also hydrodynamics[17,33−35] into the dynamic equations.

The intrinsic chemical potential is

$$\frac{\delta F}{\delta \rho_I} = -U_I + \frac{\delta F^{\mathrm{coh}}}{\delta \rho_I} + \frac{\delta F^{\mathrm{comp}}}{\delta \rho_I} \tag{12}$$

combining contributions from the ideal conformational statistics through the inverse external field functional $U_I[\rho]$, the cohesive interactions, and the compressibility term. The relation between concentration and external fields is bijective, and thus the intrinsic chemical potentials are unique functions of the concentration variables. The expression for the intrinsic chemical potential acts as a closure for the dynamic equations.

C. Numerics. The diffusion equations are integrated numerically by a Crank−Nicolson scheme on a cubic grid with 64^3 cells of mesh size h.[10] The reported simulations each take 2−3 CPU days on machines with sustained 1 Gflop/s performance. In the present model we use identical mobility coefficients $M_I = M$ and bead volume parameters $\nu_I = \nu$ for all components. The dimensionless numerical variables are

$$\theta_I(\mathbf{r}) \equiv \nu\rho_I(\mathbf{r}) \tag{13}$$

$$\phi_I \equiv \beta\mu_I(\mathbf{r}) \tag{14}$$

$$\chi_{IJ} \equiv (\beta/2\nu)[2\epsilon^0_{IJ} - \epsilon^0_{JJ} - \epsilon^0_{II}] \tag{15}$$

$$\tau \equiv kTMh^{-2}t \tag{16}$$

$$\Omega \equiv \nu^{-1}h^3 \tag{17}$$

$$d \equiv ah^{-1} \tag{18}$$

$$\kappa' \equiv \beta\kappa_H\nu \tag{19}$$

θ_I is a volume fraction field (below, θ_I is compared with the experimental weight fraction), ϕ_I is a dimensionless intrinsic chemical potential, χ_{IJ} are familiar Flory−Huggins parameters, τ is dimensionless time, Ω is a factor for noise scaling (Ω is a size-expansion parameter in Fokker−Planck theory[15,28]), d is the so-called grid scaling parameter (set to the optimal value 1.1543 in the calculations[16]), and κ' is a dimensionless compressibility parameter.[13]

A large part of the computation time is taken by so-called stencil algorithms for convolution operators with Gaussian kernels on a grid. The stencil algorithms are carefully tuned to avoid lattice artifacts.[15,16] We have found that for application to 3D problems it is crucial that grid-restricted operators conserve the proper local isotropy inherent in the continuum formulation. More details of the numerical implementation are presented in the papers.[10,15,16]

D. Parametrization. The choice of the Gaussian chain parameters is an important aspect of the method. From a practical numerical point of view it is desirable to use as few beads as possible in the polymer description since the computational time scales linearly with N. So the question is *which* short Gaussian chain to use. For the purpose of single-chain density functional calculations a "real" molecular detail polymer chain can be replaced by a Gaussian chain, provided that the response functions of Gaussian chain and molecular chain are the same. The idea is that two molecular models can be considered equivalent when they respond similarly to external perturbations. Single-chain molecular response functions or correlation functions $\langle \delta\rho_I(\mathbf{r})\ \delta\rho_J(\mathbf{r}')\rangle$ can be calculated efficiently by Monte Carlo methods.[36] Likewise, Gaussian chain response functions can be calculated analytically by the random phase approximation.[23,37]

The Monte Carlo calculation is sensitive to details of the molecular force field and is itself a topic for extensive discussion. More details of parametrization are given in ref 38 and will be published elsewhere. Here, it suffices to mention that the Monte Carlo generated structure factor of PL64 can be represented quite well by the structure factor of Gaussian chain[12] $S(\mathbf{q}) = (\Gamma^{(2)}_{\mathrm{EE}}(\mathbf{q}) - 2\Gamma^{(2)}{}_{\mathrm{PE}}(\mathbf{q}) + \Gamma^{(2)}_{\mathrm{PP}}(\mathbf{q}))^{-1}$ with composition $E_3P_9E_3$ (E is an equivalent ethylene oxide bead and P is a propylene oxide bead). This composition corresponds to monomer/bead ratios of 4.3 for the two PEO (poly(ethylene oxide)) blocks and 3.3 for the PPO (poly(propylene oxide)) block. The inverse surfactant 25R4 is modeled as $P_6E_8P_6$. We use the experimental structure factors to fit the bead size parameter a.

It is possible to parametrize mean-field interactions in self-consistent-field calculations by more refined models for monomer internal degrees of freedom.[39−41] In these calculations the smallest unit is a monomer, confined to a lattice site. From a theoretical point of view it is not difficult to translate the internal states formulation to the present continuum model. The implementation in an efficient computer program is however not straightforward. In our coarse-grained Gaussian model each bead represents a number of monomers, and the number of states would become too large for practical application. Therefore, we estimated the mean-field parameters from experimental data in an empirical fashion. The solvent−polymer interaction parameters were calculated from vapor pressure data of aqueous homopolymer solutions,[42] using the Flory−Huggins expression $\chi_{IJ} = \theta^{-2}\{\ln p/p^0 - \ln(1-\theta) - (1-1/N)\theta)\}$,[43] where p is the vapor pressure and θ is the polymer volume fraction. The equivalent number of beads N for each different homopolymer was calculated using the PL64 monomer/bead ratios given above. The empirical Flory−Huggins parameters are concentration-dependent, but we have found that in the concentration interval of interest (50−70%) the values are constant, with $\chi_{\mathrm{EO,w}} = 1.4$ and $\chi_{\mathrm{PO,w}} = 1.7$. For estimation of the EO−PO interaction parameter there are unfortunately no reliable experimental data. From group contribution methods[44] we roughly estimated a value between 3 and 5. In the simulation we used $\chi_{\mathrm{EO,PO}} = 3.0$. In the lattice-derived multiple-state mean-field models[45] the PO−EO interaction parameter is found by fitting to experimental macrophase separation diagrams. Our value is equal to the upper limit of the multiple-state model[45] and about twice larger than the average value. As we remarked

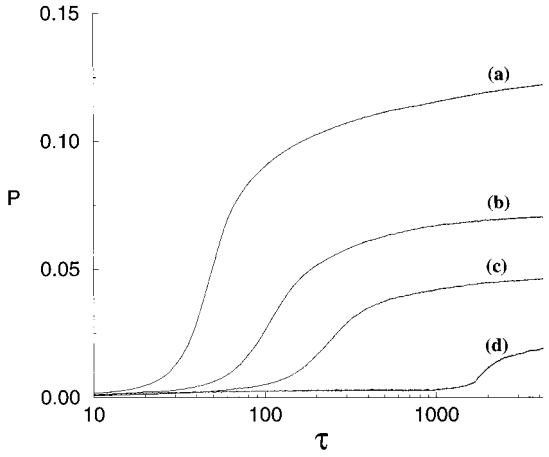

Figure 2. Time evolution of dimensionless order parameter P (see text for definition) in PL64 polymer surfactant solutions. At dimensionless time $\tau = 0$ the system is quenched from homogeneous density distribution. The labels a−d refer to simulations (Figure 1) of PL64 solution (a) 70%, (b) 60%, (c) 55%, (d) 50%.

before, in our case one bead represents several monomers, and therefore the lattice-derived multiple-state value cannot be used.

For the noise scaling parameter we have used $\Omega = 100$, and the compressibility parameter was fixed at $\kappa' = 10.0$. These values are further discussed below.

Results and Discussion

A. Pluronic L64. We performed four simulations with different PL64 concentrations, 50%, 55%, 60%, and 70% (Figures2−7). All simulations were started from an homogeneous density distributions with instantaneous quench. The phase separation dynamics is characterized by the time evolution of the average order parameter P, defined as

$$P \equiv \overline{\theta - \bar{\theta}^2} = \frac{\int_V \sum_I [\theta_I^2(\mathbf{r}) - \theta_I^{02}]\, \mathrm{d}\mathbf{r}}{V}$$

P is the mean-squared deviation from homogeneity in the system which captures both the effects of phase separation and compressibility. The time evolution of P is shown in Figure 2. The separation kinetics varies from fast spinodal crystallization (70%) to slow binodal-like nucleation (50%).

The pictures in Figure 3 are isosurface representations of θ_{PO} at dimensionless time, eq 16, $\tau = 4200$. The varying colors in the pictures denote the local concentration of the EO blocks on the isosurface of PO. The EO concentration on the PO isosurface is not constant but varies somewhat according to the microenvironment. One can clearly see several examples where the local EO concentration adjusts to accommodate defect structures. The results show that in each case the orientation of the copolymers in the self-assembly is such that the hydrophilic EO blocks shield the more hydrophobic PO block from contact with water. The observed phases are lamellar (70%, Figure 3a), bicontinuous (60%, Figure 3b), hexagonal (55%, Figure 3c), and micellar (50%, Figure 3d). The phase boundaries are a little off compared to the experimental results[3] (Figure 1), but otherwise the model reproduces the experimental phase behavior very well. The morphologies in Figure 3 consist of many clusters of different orientations. We demonstrate these clusters in Figure 4 by zooming in on small details of Figure 3.

Figure 5a shows the variation of the total density $\theta_{EO} + \theta_{PO} + \theta_w$ in the lamellar system. Depicted is the density pattern in a 2D cut through the center of the simulation box. In the regular areas the lamellae are oriented at a certain angle with respect to the normal, and in defect areas the lamellae are twisted. The total density follows the lamellar structure (Figure 5b), but with additional features. In a homogeneous system with no mesoscale structures, the total density would vary around unity in a random fashion. Here, in the inhomogeneous system there are two additional systematic effects: (i) In interfacial regions the total density decreases to values below unity.[13] By doing so, the system minimizes the unfavorable contact between adjoining phases. In Figure 5a this effect can be seen in the interface between the EO and PO blocks as a distinct grainy dark region between the white phase of the PO blocks and the complementary gray phase of EO and solvent. (ii) One phase can be compressed at the expense of the other. Here, the PO block phase is slightly compressed to an average density larger than unity, and the EO and solvent phase are slightly expanded to an average density smaller than unity. The magnitude of the random fluctuations, the size of the interfacial dip, and the phase compression/expansion are controlled by the value for the compressibility parameter. The exact relation is rather complicated, since there are additional couplings with the values for the Flory−Huggins parameter and the length of the polymer.[46] In other simulations we found that the random fluctuation in homogeneous systems drops below 1% using a compressibility parameter of $\kappa' = 20$, keeping all other parameters the same. The variation of the total density fluctuation in all presented simulations is a few percent. This seems reasonable, but we have no experimental verification.

It is important to realize to what extent the simulated instantaneous quench from homogeneous density distribution resembles the experimental conditions. The time scale of phase separation is only roughly known. The experimental microphase structures are determined after hours, days, or even weeks of equilibration time, while sometimes the phase separation kinetics is accelerated by repeated centrifugation.[3] The microviscosity of bulk PPO 750 is about 66 cP at 35 °C; the microviscosity of PEO−PPO micellar cores is also of this order of magnitude.[47] Combining these values with the Stokes−Einstein relations (using bead size a 1.5−1.9 nm, see below) gives a reasonable estimate for the total time span of the simulations in the milliseconds−seconds range.

Detailed analysis of the structure factors (Figure 6) shows that all primary diffraction peaks are located at the same frequency ($q_0 = 0.17h^{-1}$), while the experimental SAXS data show a variation in the repeat distance from 7.5 nm (68%) to 9.1 nm (53%).[3] The additional coarsening found in the experimental micellar system might be attributed to slow relaxation. In temperature-jump experiments it was found that PEO−PPO−PEO micelles rearrange in two stages.[48] First there is a relatively fast stage in the tens of microseconds to millisecond range, in which individual polymer molecules escape and reinsert in the micelles. The micellar size distribution changes in the second slower

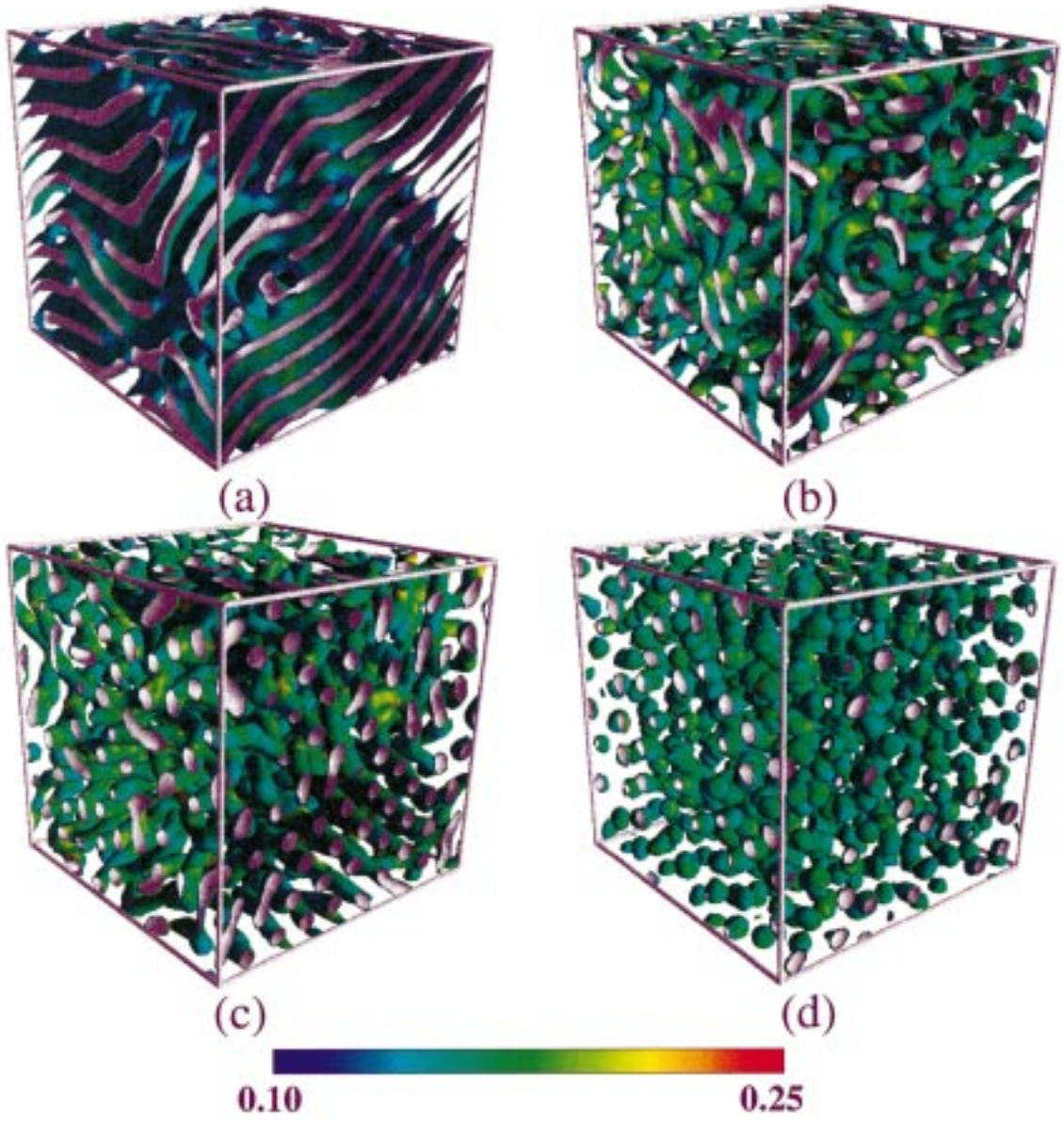

Figure 3. Snapshots of mesoscale structures in Pl64 polymer surfactant solutions at dimensionless time $\tau = 4200$. θ_{PO} isosurfaces with θ_{EO} surface distribution in color. (a) 70%, isolevel $\theta_{PO} = 0.59$, (b) 60%, isolevel $\theta_{PO} = 0.5$, (c) 55%, isolevel $\theta_{PO} = 0.46$, (d) 50%, isolevel $\theta_{PO} = 0.42$. θ_{EO} as indicated in the color legend. The labels a−d refer to simulations (Figure 1) of PL64 solution (a) 70%, (b) 60%, (c) 55%, (d) 50%.

stage between 1 and 100 ms. Although the time scale of events is similar to the scale calculated with the Stokes−Einstein relation referred to above, one must realize that the simple diffusion model we have used here does not include convective effects. In an earlier paper we have shown that the model can be extended to include hydrodynamic effects.[17] We will study convection more thoroughly in the future.

So far, the bead size a is still an unknown (adjustable) parameter, to be fitted to experiment. The effective value of the mesh size h can be calculated by equating the experimentally determined periodicity and the theoretical repeat distance hq_0^{-1} of the mesoscale structures. We find that the mesh size is not entirely constant but varies somewhat from $h = 1.3$ nm (70%) to $h = 1.6$ nm (55%). Using the grid-scaling ratio $d \equiv ah^{-1} = 1.1543$, we can now calculate that the effective Gaussian chain bead size varies between 1.5 nm (70%) and 1.9 nm (55%). It is illustrative to compare the bead size with simple molecular models. A fully stretched unit of 3.8 monomers (average of monomer/bead ratios for EO and PO) with each bond in the same direction has a length of 1.7 nm (calculated using $l_{C-O} = 0.143$ nm and $l_{O-O} = 0.153$ nm). A fully disordered unit with each bond in a random orientation has a root-mean-square length 0.5 nm. These numbers are comparable to the values of a we found. But one must be careful to interpret the value of a as an indicator for local

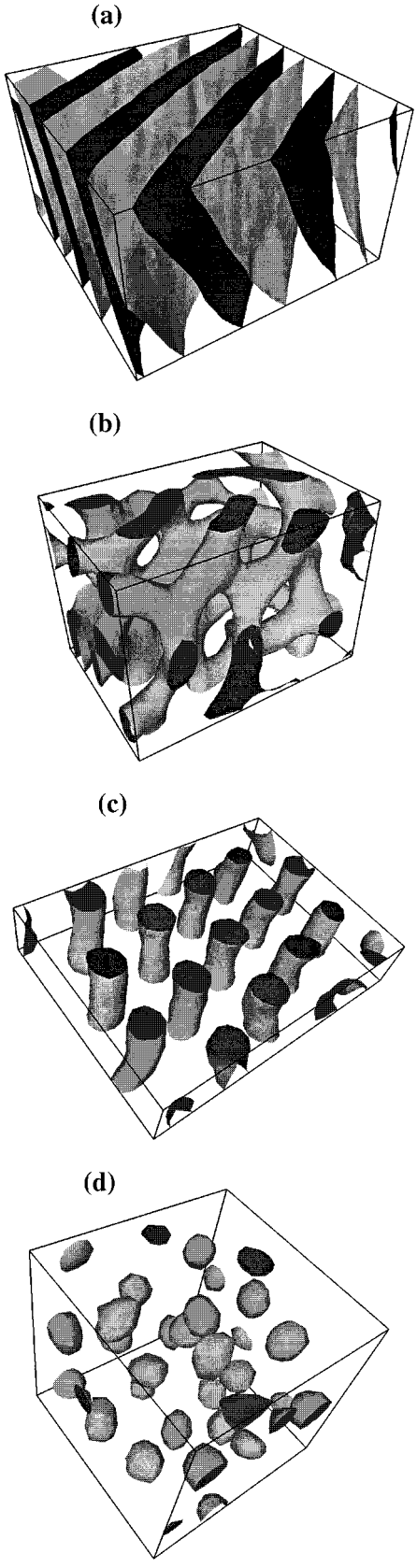

Figure 4. Enlarged small parts of snapshots from Figure 3. Mesophases at different concentrations of Pl64: (a) 70%, lamellar phase; (b) 60%, bicontinuous; (c) 55%, cylindrical; (d) 50%, micellar phase.

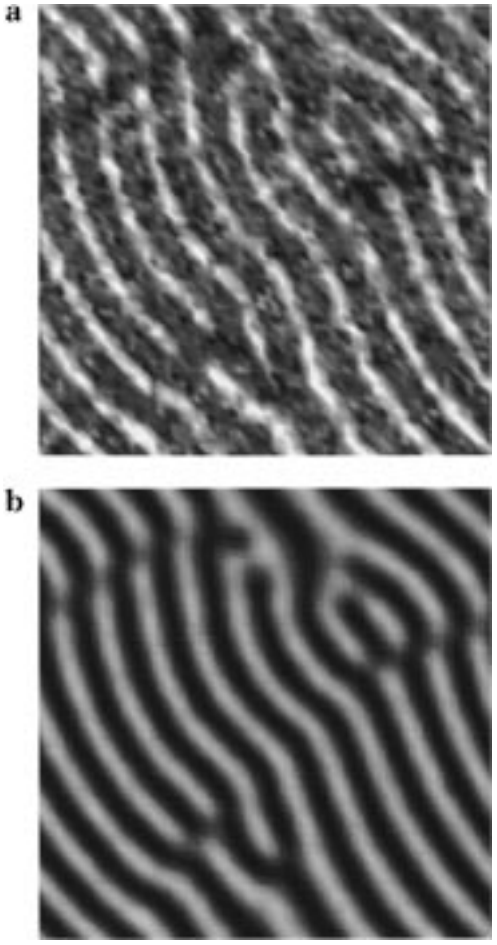

Figure 5. Variation of density in 70% Pl64 solution at dimensionless time $\tau = 4200$. 2D cut through the middle of the box shown in Figure 3a. (a) Total density $\theta_{EO} + \theta_{PO} + \theta_w$ (linear gray scale 0.97 black to 1.03 white), (b) density θ_{PO} (linear gray scale 0.03 black to 0.97 white).

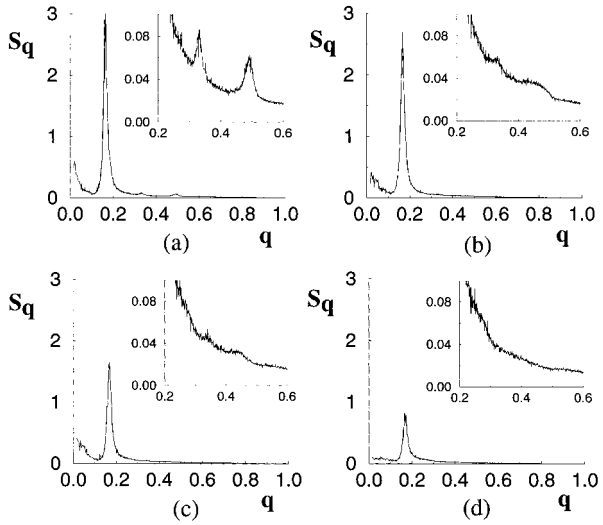

Figure 6. Structure factors of Pl64 solutions at dimensionless time $\tau = 4200$. Data the same as in Figure 3. Each graph was obtained by performing a 3D Fourier transform of $\theta_{PO}(\mathbf{r})$ and subsequent averaging over all directions. Units on the horizontal axis are h^{-1}; units on the vertical axis are arbitrary (but the same for all four systems).

molecular structure. A more precise comparison, using the Monte Carlo calculations for the structure factor mentioned in the previous section, corresponds to $a \simeq 1.3-1.5$ nm.[38] The empirical values are fairly independent of solvent conditions, so a single-size bead model is apparently sufficient to describe the PL64 system. Below, we will show that the inverse block sequence

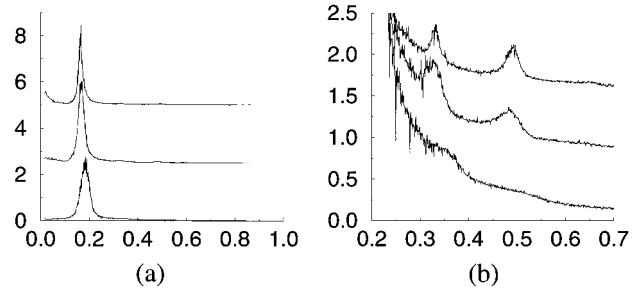

Figure 7. Time evolution of structure factor in 70% Pl64 solution. At $\tau = 0$ the system is quenched from homogeneous density distribution (simulation a in Figure 2). Dimensionless times $\tau = 50$ (bottom), $\tau = 500$ (middle), and $\tau = 4200$ (top). Units on the horizontal axis are h^{-1}. Units on the vertical axis are arbitrary. The graphs have been shifted vertically for clarity.

polymer 25R4 has approximately the same effective bead size.

The total simulation box measures about 90 nm on each side with a total box volume of 7.3×10^5 nm^3. In the language of molecular simulations, a box of pure water with this size contains 2.3×10^7 molecules of water; a box of pure polymer contains 1.5×10^5 surfactant molecules. The simulations clearly probe the scale of mesoscopic phenomena.

In the structure factor of the micellar phase (50%) there is a higher-order Bragg peak at $1.59-1.70q_0$, indicative of weak ordering, but the effect is very small; see also Figure 4d. In the hexagonal phase (55%) there are harmonics at $2q_0$ and $\sqrt{7}q_0$. The expected peak at $\sqrt{3}q_0$ is missing, probably because of the relatively broad primary peak. The final structure of this system clearly has microdomains of high hexagonal order (Figure 4c). However, the global long-range order is not yet established (Figure 3c), which causes a smeared picture of Bragg peaks. Continuing of simulation would improve ordering, but the long-range hexagonal ordering can be induced much faster by application of shear flow.[20] In the structure factor of the 60% solution there is a harmonic at $2q_0$ and a broad shoulder at $2.35-2.9q_0$. The lamellar phase (70%) has well-developed second- and third-order peaks at $2q_0$ and $3q_0$, respectively. There is a boundary region connecting the different lamellar microdomains which themselves have almost no defects (Figure 4a).

We performed a cluster analysis according to an algorithm that selects all neighboring cells with volume fraction θ_{PO} higher than a supplied threshold value. From the resulting clusters we analyzed the topology in order to determine whether the structures were percolating the simulation box. Applied to the 60% solution, using the threshold value $\theta_{PO} = 0.6$, we found that both PO- and EO-rich domains coagulate into one percolating cluster. Therefore, this phase is bicontinuous. It is not possible to deduce the type of bicontinuous phase (gyroid, double diamond, etc.) from the structure factors or 3D concentration fields since there are too many defects. However, the enlarged view (Figure 4b) of domain morphology from Figure 3b clearly indicates formation of a pattern with gyroid-type symmetry. As the structure is still very much deformed, the symmetry cannot be extracted from the structure factor.

The time evolution of the structure factor of the lamellar phase is shown in Figure 7. The simulations make two main effects visible which are of general interest. First, after the quench the primary peak shifts

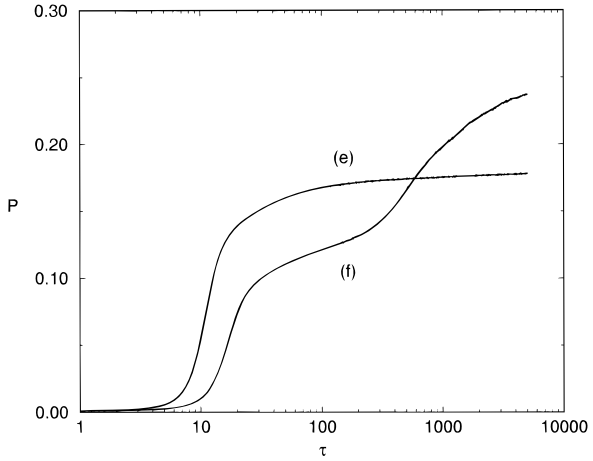

Figure 8. Time evolution of dimensionless order parameter P in 25R4 polymer surfactant solutions. At dimensionless time $\tau = 0$ the system is quenched from homogeneous density distribution. The labels e−f refer to the simulations (Figure 1) of 25R4 solution: (e) 70%, (f) 60%.

to a lower value, reflecting an increase in thickness of the lamellae. Second, the harmonic peaks at $2q_0$ and $3q_0$ continue to grow, while the main order parameter hardly changes with time anymore (Figure 2). The physical picture is that in the first stages of phase separation the system is still isotropic with one RPA peak in the structure factor. Then slowly small patches of oriented lamellae develop, which grow by a defect annihilation mechanism.

In the following paper in this series we will report the analysis for a sheared Pluronic system.[20] In an earlier paper we have already shown that application of shear has a pronounced effect on 3D mesoscale structure formation in diblock polymer melts.[18,19] The orientation of the structures is much faster, and the final structures are more perfect.

B. Pluronic 25R4. We also studied solutions of the Pluronic 25R4, with the inverse block structure hydrophobic−hydrophilic−hydrophobic. The equivalent Gaussian chain is now $P_6E_8P_6$; all other parameters were the same as in the PL64 simulations.

The time evolution of the order parameters is shown in Figure 8. Compared to the PL64 solutions, the phase separation is faster. This is not surprising, since 25R4 is overall more hydrophobic than PL64, and in solutions of the same concentration we therefore expect that the thermodynamic driving forces for phase separation are larger. In the 60% solution we observe a distinct double step, corresponding to the nucleation of small water droplets. Interestingly, the nucleation starts *after* the initial formation of a lamellar phase.

The isosurface patterns are shown in Figure 9. The results are in good agreement with experiment (Figure 1). In the 70% 25R4 solution (Figure 9e) we observe the formation of the lamellar phase. The 70% Pl64 is also lamellar (see previous section). Thus, we confirm the experimental observation that the lamellar phase formation is independent of sequence. It is known that in the more diluted 25R4 solutions mesoscale structures (bicontinuous, hexagonal, or micellar phases) are absent.[49] In our simulations of solutions with 25R4 surfactant concentration 40% and lower we did not observe any mesoscale structure formation whatsoever. It is easy to understand why upon dilution the inverse block sequence 25R4 does not form the same mesoscale structures as in the PL64 solutions. In a less concen-

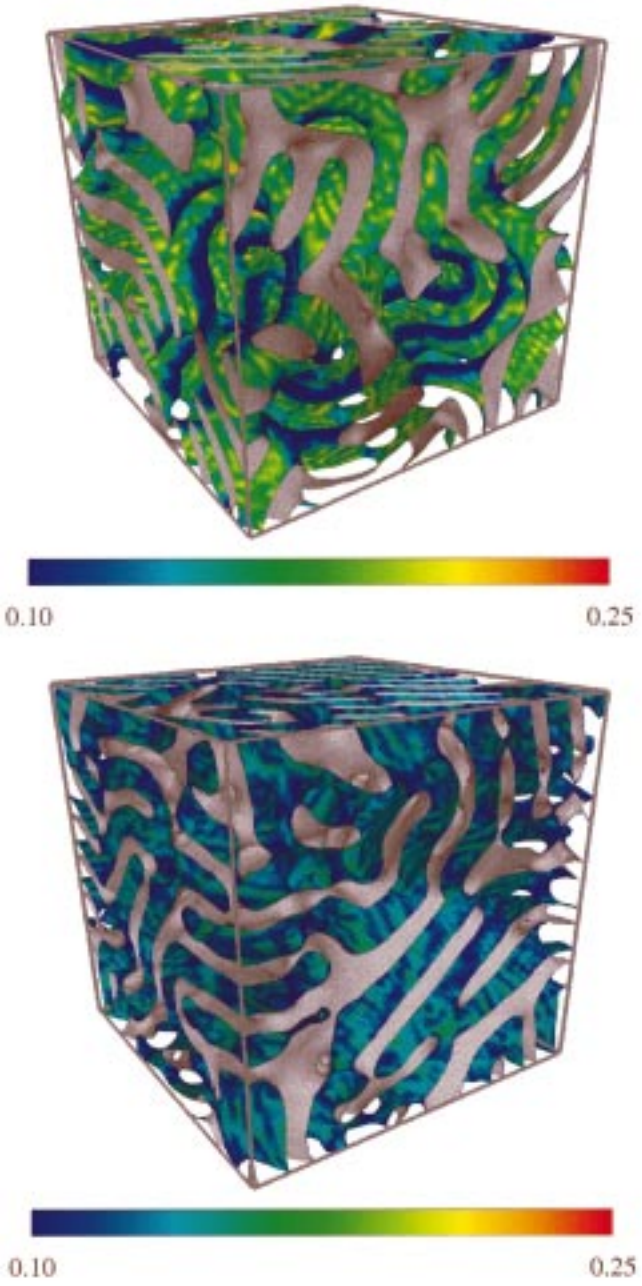

Figure 9. Snapshots of mesoscale structures in 25R4 polymer surfactant solutions at dimensionless time $\tau = 5000$. θ_{PO} isosurfaces with θ_{EO} surface distribution in color. (e, top) 70% 25R4, isolevel $\theta_{PO} = 0.59$, (f, bottom) 60% 25R4, isolevel $\theta_{PO} = 0.52$. θ_{EO} as indicated in color legend. The labels e−f refer to the simulations (Figure 1) of 25R4 solution: (e) 70%, (f) 60%.

trated system, self-assembled 25R4 molecules would be forced to each orient *two* hydrophobic blocks toward the inside of a surfactant aggregate. The loss in configurational freedom is so high that self-assembly is prevented, and the system remains continuous. But overall, 25R4 is quite hydrophobic, and if the hydrophilic blocks cannot shield the hydrophobic blocks from contact with water, then there is the possibility of macrophase separation. This explains the formation of the small water droplets, dispersed throughout the system in the 60% 25R4 solution (Figure 9f). In the experimental phase diagram there is an indication of a small two-phase region of water-rich phase and lamellar phase (L_1 + L_α) near 60% surfactant concentration. The mixed droplet−lamellar phase system we have found in the

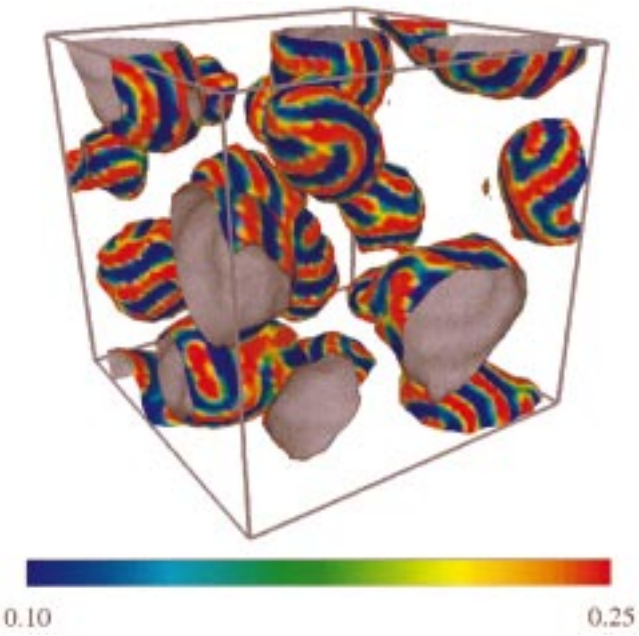

Figure 10. Snapshot of dispersed water droplet mesoscale structure in 25R4 polymer surfactant 60% solution at dimensionless time $\tau = 5000$. θ_w isosurface (isolevel 0.56) with θ_{EO} surface distribution in color (indicated as in color legend). Orientation of the snapshot is the same as in Figure 9f.

simulation corresponds to this experimental two-phase region.

An interesting result is that in the 60% 25R4 solution the lamellae are oriented perpendicular toward the water droplets surfaces (Figure 10). Depicted is the distribution of small water droplets, with θ_{EO} as a coloring for the droplets surfaces. The concentration of water inside the droplets is $\theta_w > 0.56$. In 1D polymer adsorption models one often assumes a layering parallel to the surface.[50] Applied to the droplets, this would mean a stuffed "onion" model in which the lamellae are oriented parallel to the surface. In such a model θ_{EO} is constant, given a certain droplet surface. From Figures 9f and Figure 10 it is evident that this is not the case: parallel orientation of lamellae is absent, and θ_{EO} varies in a "zebra-fish" pattern. Perpendicular orientation of mesoscale structures near interfaces is not uncommon in thin block copolymer films,[51] but as far as we know the effect has not yet been observed in polymer surfactant solutions. Notice that in the present system there is also confinement, since the lamellar solution is locked between the dispersed droplets. It would be interesting to see whether experiments can verify the simulation results.

Here, we have interpreted the water droplets as indication for macrophase separation, in agreement with the experimental phase diagram. However, an alternative view of the same system is that of a perforated lamellar mesophase, where the pores are filled with solvent. If this is the case, then the dispersed droplets may be thermodynamically stable, and macrophase separation will not occur.

This points to a general observation. We find that these polymer surfactant systems exhibit a bewildering variety of structured phases. From inspection of a simulated complex curved 3D density field, it is by no means always clear what type of mesophase the system is trying to form. Especially in phase boundary regions nonequilibrium phases with very complex bicontinuous geometry seem to be the rule rather than the exception.

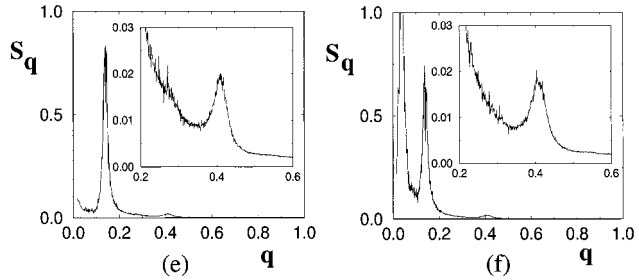

Figure 11. Structure factors of 25R4 solutions at dimensionless time $\tau = 5000$. Data the same as in Figure 9. Units on the horizontal axis are h^{-1}; units on the vertical axis are arbitrary. Labels e−f refer to the simulations (Figure 1) of 25R4 solution: (e) 70% and (f) 60%.

The structure factor of the lamellar phase is depicted in Figure 11. The primary peak is at $q_0 = 0.14\ h^{-1}$. If we use the same mesh size as established for the PL64 system ($h = 1.3-1.6$ nm), the calculated repeat distance is 9.3−11.4 nm. Experimentally, the repeat distance is 7 nm.[49] Alternatively, if we match experimental and calculated values of the repeat distance, as in the case of the PL64 solutions, we can now also calculate the effective mesh size $h = 1$ nm and bead size parameter $a = 1.2$ nm. The agreement between PL64 and 25R4 values is reasonable, which is further proof that the Gaussian chain model is sufficient to capture the phase separation phenomenon in a semiquantitative way.

C. General Remarks. *Thermal Noise.* In the presented simulations the thermal noise is a small perturbation of a few percent imposed on large systematic thermodynamic forces. This is as it should be since functional Langevin theory only applies if each coarse-grained cell contains a sufficient number of degrees of freedom.[28] The higher this number, the larger the noise scaling parameter Ω and the smaller the amplitude of the noise (the noise amplitude scales as $\Omega^{-1/2}$). In practice, we have found from many more simulations of similar copolymer systems that the noise is relatively unimportant for size and shape of the mesoscale structures—provided Ω is chosen large. However, from a theoretical point of view there remain many interesting questions relating to the role of thermal fluctuations in coarse-grained models. An intriguing and by no means resolved problem is the quantitative definition of "degree of freedom". The formula $\Omega = \nu^{-1}h^3$ referred to in the list of dimensionless variables (eq 17) is based on a very crude model in which each Gaussian bead in a polymer chain represents one degree of freedom. If we now use a reasonable value for the bead molecular volume $\nu \simeq 0.3$ nm^3 (based on the density of pure Pluronic) and mesh size $h = 1.4$ nm, we can easily calculate that $\Omega \approx 9$. On the other hand, if we assume that each solvent molecule represents one degree of freedom, then $\Omega \lesssim 90$ since each cell contains maximally this number of water molecules in water-rich regions. However, the right choice for Ω is not so obvious as these simple calculations suggest. A more sophisticated model describes the collapse of freedom going from molecular detail to a coarse-grained model by matching of response functions.[38]

Gaussian Chain Approximation. The Gaussian chain approximation does not mean that the polymers are represented as *ideal* random coils. Rather, the external potentials "squeeze" the conformational distribution function in such a way that the polymer statistics is that of an elongated structure. The topic of conformational analysis and the molecular interpretation will be addressed much more thoroughly in the following paper in the series. In the presented microphase morphologies, on the average a polymer molecule is extended two to four times with respect to isotropic random coil. The extension depends, of course, on the position of the polymer molecule with respect to the self-assembly interface. We believe that the Gaussian chain approximation is justified not only from the analysis of conformations but also, in a more practical manner, from the very good agreement with the experimental phase diagram. In an earlier paper[52] we have tried to apply the method to low molecular weight lipids, but with only modest results. The Pluronics molecules are relatively large and flexible surfactants. Clearly, application of the method becomes better the larger and more flexible the molecules are.

Geometrical and Conformational Analysis. An important quantity for characterization of the mesoscale structures is the surface per molecule $a_p = A/N_p$, where A is the surface area of the interface and N_p the number of polymer molecules. a_p can be calculated from experimental structure factors and simple models for the interface.[3,49,53] For example, for a lamellar structure $a_p = \nu_p/(d\Phi_p)$ where d is the repeat distance obtained from the position of the main peak in the SAXS spectrum and Φ_p the polymer volume fraction. In principle, we can also analyze our results this way, since we know the structure factor and the volume fraction of polymer. But since we have calibrated the effective Gaussian bead size on the experimental structure factors, we cannot gain much additional information beyond the original analysis of the experimental data. It is more interesting to calculate the surface per molecule directly from the plots of simulated 3D isosurfaces and observe how the polymer molecule is extra compressed or elongated near defect areas and in the different phases. Some configurations of polymer molecules connect different aggregates by bridging; other configurations loop back in the same aggregate.[49] For such a sophisticated analysis we need a good definition of interface, a means to calculate the surface area of an arbitrarily curved interface,[54] and also knowledge about the two- and three-body correlators of the polymer molecule.[19] These issues will be discussed extensively in a following paper.

Dynamic Model. Many variations of the model are possible with respect to the choice for the kinetic coefficients.[14,30−32] Previously, we have shown how spinodal phase separation dynamics in diblock copolymer melts can be simulated using nonlocal kinetic coefficients (Rouse or reptation) by so-called external potential dynamics models.[14] At this moment it is not yet clear to what extent nonlocal kinetic coefficients models can or should be applied to solutions of polymer surfactants. From the simulations it is evident that after quench from homogeneous density distribution the phase separation dynamics proceeds in two stages. In the first stage fluctuations with a length scale of the polymer coil size grow rapidly in binodal- or spinodal-like fashion, depending on conditions. In the second stage, which is much slower, phases grow by collective rearrangement phenomena on a length scale larger than the coil size of the polymer. The precise spectrum of the kinetic coefficient is relatively unimportant for the second slower stage. It is straightforward to introduce different mobilities for polymer and solvent in the present model.

In this paper we have discussed collective relaxation by diffusional processes only. On even longer time scales than we have studied here convection will start to contribute to the phase separation dynamics. One can imagine that convective effects are especially important in the more dilute solutions. In a mesoscale structured concentrated solution the aggregate structures themselves shield the flow (because they are more viscous than the surrounding medium), in such a way that with respect to hydrodynamics the morphology effectively behaves as a porous medium. Extensions of the dynamic density functional model with hydrodynamics[17] and shear effects[18,19] have been demonstrated already. The application to Pluronic solutions can be found in ref 20.

Conclusion

We have presented an application of the dynamic mean-field density functional method to the phase behavior of aqueous solutions of triblock polymer surfactant (ethylene oxide)$_{13}$(propylene oxide)$_{30}$(ethylene oxide)$_{13}$ and (propylene oxide)$_{19}$(ethylene oxide)$_{33}$-(propylene oxide)$_{19}$. This is the *first* mesoscale model for specific complex polymer solutions with coarse-grained 3D resolution of the dynamic morphology formation.

The idea behind the method is that on a time scale, coarse-grained with respect to internal relaxation of individual polymer molecules, the conformational distribution is in local equilibrium constantly. The model describes collective relaxation by stochastic diffusion equations. The dynamics of the 3D morphologies is controlled by nonlocal thermodynamic forces, a linear diffusion operator, and thermal noise. The Pluronic solutions are modeled as a collection of Gaussian chains in a mean-field compressible environment. Using the same Gaussian chain and mean-field parameters, we describe the phase formation of the two surfactants in a range of solvent conditions. The results are in very good agreement with experiment. In (ethylene oxide)$_{13}$-(propylene oxide)$_{30}$(ethylene oxide)$_{13}$ solutions, we find in a small concentration interval 50−70% the four classical morphologies: lamellar phase (70%), bicontinuous phase (60%), hexagonal phase (55%), and micellar phase (50%). In solutions of the inverse block sequence (propylene oxide)$_{19}$(ethylene oxide)$_{33}$(propylene oxide)$_{19}$ we find a lamellar phase (70%) and a continuous phase (40%). There is a region of two-phase coexistence at 60%, with tiny water droplets dispersed throughout the system. In the two-phase system lamellae are oriented perpendicular to the water droplets.

The dynamic mean-field density functional model is very flexible and can be extended in many different directions. The calculation method is well suited for the description of microphase separation phenomena in a wide variety of complex polymer systems.[9−20]

Acknowledgment. A.V.Z. and G.J.A.S. acknowledge the support of the ESPRIT project MESODYN No. EP 22685 of the European Commission. We thank Jan Kraak for assistance with visualization.

References and Notes

(1) Lodge, T. P.; Muthukumar, M. *J. Phys. Chem.* **1996**, *100*, 13275−13292.
(2) Alexandridis, P.; Hatton, T. A. *Colloids Surf. A* **1995**, 1−46.
(3) Alexandridis, P.; Olsson, U.; Lindmann, B. *Macromolecules* **1995**, *28*, 7700−7710.
(4) Alexandridis, P.; Olsson, U.; Lindmann, B. *J. Phys. Chem.* **1996**, *100*, 280−288.
(5) Cross, M. C.; Hohenberg, P. C. *Rev. Mod. Phys.* **1993**, *65*, 851−1112.
(6) Cahn, J. W.; Hilliard, J. E. *J. Chem. Phys.* **1958**, *28*, 258−267.
(7) Oono, Y.; Puri, S. *Phys. Rev. Lett.* **1987**, *58*, 836−839.
(8) de Gennes, P. G. *J. Chem. Phys.* **1980**, *72*, 4756−4763.
(9) Fraaije, J. G. E. M. *J. Chem. Phys.* **1993**, *99*, 9202−9212.
(10) Fraaije, J. G. E. M.; van Vlimmeren, B. A. C.; Maurits, N. M.; Postma, M.; Evers, O. A.; Hoffmann, C.; Altevogt, P.; Goldbeck-Wood, G. *J. Chem. Phys.* **1996**, *106*, 4260−4269.
(11) Maurits, N. M.; Zvelindovsky, A. V.; Fraaije, J. G. E. M. *J. Chem. Phys.* **1998**, *108*, 2638−2650.
(12) Maurits, N. M.; Fraaije, J. G. E. M. *J. Chem. Phys.* **1997**, *106*, 6730−6743.
(13) Maurits, N. M.; van Vlimmeren, B. A. C.; Fraaije, J. G. E. M. *Phys. Rev. E* **1997**, *56*, 816−825.
(14) Maurits, N. M.; Fraaije, J. G. E. M. *J. Chem. Phys.* **1997**, *107*, 5879−5889.
(15) van Vlimmeren, B. A. C.; Fraaije, J. G. E. M. *Comput. Phys. Commun.* **1996**, *99*, 21−28.
(16) Maurits, N. M.; Altevogt, P.; Evers, O. A.; Fraaije, J. G. E. M. *Comput. Theor. Polym. Sci.* **1996**, *6*, 1−8.
(17) Maurits, N. M.; Zvelindovsky, A. V.; Sevink, G. J. A.; van Vlimmeren, B. A. C.; Fraaije, J. G. E. M. *J. Chem. Phys.* **1998**, *108*, 9150−9154.
(18) Zvelindovsky, A. V.; Sevink, G. J. A.; van Vlimmeren, B. A. C.; Maurits, N. M.; Fraaije, J. G. E. M. *Phys. Rev. E* **1998**, *57*, R4699−R4702.
(19) Zvelindovsky, A. V.; Sevink, G. J. A.; van Vlimmeren, B. A. C.; Maurits, N. M.; Fraaije, J. G. E. M. *Prog. Colloid Polym. Sci.* **1998**, *110*, 251−254.
(20) Zvelindovsky, A. V. M.; van Vlimmeren, B. A. C.; Sevink, G. J. A.; Maurits, N. M.; Fraaije, J. G. E. M. *J. Chem. Phys.* **1998**, *109*, 8751−8754.
(21) Kawakatsu, T. *Phys. Rev. E* **1997**, *56*, 3240−3250.
(22) Hasegawa, R.; Doi, M. *Macromolecules* **1997**, *30*, 3086−3089.
(23) de Gennes, P.-G. *Scaling Concepts in Polymer Physics*; Cornell University: Ithaca, NY, 1979.
(24) Doi, M.; Edwards, S. F. *The Theory of Polymer Dynamics*; Clarendon: Oxford, 1986.
(25) Noolandi, J.; Shi, A.-Ch.; Linse, P. *Macromolecules* **1996**, *29*, 5907−5919.
(26) Janert, Ph. K.; Schick, M. *Macromolecules* **1997**, *30*, 137−144.
(27) Fraaije, J. G. E. M.; van Vlimmeren, B. A. C.; Maurits, N. M.; Postma, M.; Evers, O. A.; Hoffmann, C.; Altevogt, P.; Goldbeck-Wood, G. *J. Chem. Phys.* **1997**, *106*, 4260−4269.
(28) Van Kampen, N. G. *Stochastic Processes in Physics and Chemistry*; North-Holland: Amsterdam, 1992.
(29) Gardiner, C. W. *Handbook of Stochastic Methods*; Springer: Berlin, 1990.
(30) Kawasaki, K.; Sekimoto, K. *Physica* **1987**, *143A*, 349−413.
(31) Kawasaki, K.; Sekimoto, K. *Physica* **1988**, *148A*, 361−413.
(32) Kawasaki, K.; Sekimoto, K. *Macromolecules* **1989**, *22*, 3063−3075.
(33) Koga, T.; Kawasaki, K. *Phys. Rev. A* **1991**, *44*, R817−R820.
(34) Kawakatsu, T.; Kawasaki, K.; Furusaka, M.; Okabayashi, H.; Kanaya, T. *J. Chem. Phys.* **1993**, *99*, 8200−8217.
(35) Valls, O. T.; Farrell, J. E. *Phys. Rev. E* **1993**, *47*, R36−R39.
(36) Wanyne, M. L.; Suter, U. W. *Conformational Theory of Large Molecules*; John Wiley & Sons: New York, 1994.
(37) Leibler, L. *Macromolecules* **1980**, *13*, 1602−1617.
(38) van Vlimmeren, B. A. C. Mesoscopic Dynamics. Simulation of Microphase Separation in Complex Fluids. Ph.D. Thesis, University of Groningen, 1998.
(39) Hurter, P. N.; Scheutjens, J. M. H. M.; Hatton, T. A. *Macromolecules* **1993**, *26*, 5030−5040.
(40) Hurter, P. N.; Scheutjens, J. M. H. M.; Hatton, T. A. *Macromolecules* **1993**, *26*, 5592−5601.
(41) Linse, P.; Hatton, T. A. *Langmuir* **1997**, *13*, 4066−4078.
(42) Malcolm, G. N.; Rowlinson, J. S. *Trans. Faraday Soc.* **1957**, *53*, 921−931.
(43) Hill, T. L. *An Introduction to Statistical Thermodynamics*; Addison-Wesley: Reading, MA, 1962.
(44) Krevelen, D. W. *Properties of Polymers, Their Correlation with Chemical Structure; Their Numerical Estimation and Prediction from Additive Group Contribution*; Elsevier: Amsterdam, 1990.
(45) Malmsten, M.; Linse, P.; Zhang, K.-W. *Macromolecules* **1993**, *26*, 2905−2910.

(46) Wu, D. T.; Fredrickson, G. H.; Carton, J.-P.; Ajdari, A.; Leibler, L. *J. Polym. Sci., Part B: Polym. Phys.* **1995**, *33*, 2373−2389.
(47) Nvaggioli, T.; Tsao, B.; Alexandridis, P.; Hatton, T. A. *Langmuir* **1995**, *11*, 119−126.
(48) Goldmints, I.; Holzwarth, J. F.; Smith, K. A.; Hatton, T. A. *Langmuir* **1997**, *13*, 6130−6134.
(49) Alexandridis, P.; Olsson, U.; Lindman, B. *J. Phys. Chem.* **1996**, *100*, 280−288.
(50) Fleer, G. J.; Cohen Stuart, M. A.; Scheutjens, J. M. H. M.; Cosgrove, T.; Vincent, B. *Polymers at Interfaces*; Chapman Hall: London, 1993.
(51) van Dijk, M. A.; van den Berg, R. *Macrmolecules* **1995**, *28*, 6773−6778.
(52) van Vlimmeren, B. A. C.; Postma, M.; Huetz, P.; Brisson, A.; Fraaije, J. G. E. M. *Phys. Rev. E* **1996**, *54*, 5836−5839.
(53) Alexandridis, P.; Olsson, U.; Lindman, B. *Langmuir* **1998**, *14*, 2627−2638.
(54) Jinnai, H.; Koga, T.; Nishikawa, Y.; Hashimoto, T.; Hyde, S. T. *Phys. Rev. Lett.* **1997**, *78*, 2248−2251.

MA980947+